Classification: BIOLOGICAL SCIENCES, Neuroscience

Synaptotagmin Oligomerization is Essential for Calcium Control of Regulated Exocytosis

Oscar D. Bello[a,b,1], Ouardane Jouannot[a,1], Arunima Chaudhuri[a], Ekaterina Stroeva[a], Jeff Coleman[a], Kirill E. Volynski[b], James E. Rothman[a,b,2] & Shyam S. Krishnakumar[a,b,2]

[a]Department of Cell Biology, Yale University School of Medicine, 333 Cedar St, New Haven, CT, 06520, USA.

[b]Department of Clinical and Experimental Epilepsy, Institute of Neurology, University College London, Queens Square House, WC1N 3BG, London, UK.

[1]O.D.B and O.J. contributed equally to this work.

[2]To whom correspondence should be addressed:

Shyam S. Krishnakumar
Department of Cell Biology,
Yale University School of Medicine
333 Cedar St, New Haven, CT 06520
Tel: (203) 737-3810
Email: shyam.krishnakumar@yale.edu

James E. Rothman
Department of Cell Biology
Yale University School of Medicine
333 Cedar St, New Haven, CT 06520
Tel: (203) 737-5293
Email: james.rothman@yale.edu.

K*eywords*:

Regulated exocytosis, Synaptotagmin, SNARE protein, calcium, PC12 cells, pHluorin

ABSTRACT

Regulated exocytosis, which underlies many intercellular signaling events, is a tightly controlled process often triggered by calcium ions (Ca^{2+}). Despite considerable insight into the central components involved, namely the core fusion machinery (soluble N-ethylmaleimide–sensitive factor attachment protein receptor, SNARE) and the principal Ca^{2+} sensor (C2 domain proteins, like Synaptotagmin), the molecular mechanism of Ca^{2+}-dependent release has been unclear. Here we report that the Ca^{2+}-sensitive oligomers of Synaptotagmin1, a conserved structural feature among several C2 domain proteins, play a critical role in orchestrating Ca^{2+}-coupled vesicular release. This follows from pHluorin-based imaging of single vesicle exocytosis in pheochromocytoma (PC12) cells showing that selective disruption of Synaptotagmin1 oligomerization using a structure-directed mutation (F349A) dramatically increases the normally low-levels of constitutive exocytosis to effectively occlude Ca^{2+}-stimulated release. We propose a parsimonious model whereby Ca^{2+}-sensitive oligomers of Synaptotagmin (or similar C2 domain protein) assembled at the site of docking physically block spontaneous fusion, until disrupted by Ca^{2+}. Our data further suggests Ca^{2+}-coupled vesicular release is triggered by the removal of the inhibition, rather than a direct activation of the fusion machinery.

SIGNIFICANCE

Synaptotagmin is the primary Ca^{2+}-sensor for regulated exocytosis. It couples Ca^{2+}-binding to SNARE-catalyzed fusion, but how this happens is unclear. Here, using a targeted mutation combined with a single vesicle fusion optical assay, we show that the recently discovered structural feature of Synaptotagmin to self-oligomerize is essential for Ca^{2+}-coupling of vesicular fusion. This suggests a novel yet simple model in which these Synaptotagmin oligomers formed at the interface of the docked vesicle physically preventing fusion, until the influx of Ca^{2+}.

\body

Timely secretion of a variety of critical molecules, including neurotransmitters, hormones and enzymes, are achieved via regulated exocytosis (1-3). During regulated exocytosis, the secretory vesicles fuse to the plasma membrane (PM) in response to an external stimuli, typically activated by Ca^{2+} influx. However, SNARE proteins, which catalyze the fusion of the cargo-carrying vesicles, are constitutively active (4, 5). When the cognate pair of SNAREs located on the vesicle (v-SNARE) and the target membrane (t-SNARE) are in molecular proximity, they readily assemble into a stable complex providing the energy to fuse the membranes (4, 5). Thus, regulated exocytosis requires mechanisms both to prevent the spontaneous fusion of vesicles ('clamping') under rest and to transduce the Ca^{2+} signal into activating the clamped fusion machinery (1-3).

Synaptotagmins (Syt), a family of tandem C2-domain (C2A & C2B) containing protein that bind both Ca^{2+} ions and SNARE proteins (3, 6-10), play a critical role in this processes. The Ca^{2+} activation mechanism has been well-characterized and involves the insertion of surface loops on each of the C2 domains into the membrane bilayer with Ca^{2+} coordinating it to acidic lipids, phosphatidylserine (PS) and phosphatidylinositol 4,5-bisphosphate (PIP2) (11-16). But, how the constitutive fusion is arrested to enable the Ca^{2+}-coupled exocytosis is not known. Nevertheless, Syt is believed to play a crucial role in this process as deletion (or mutations) of Syt1 (the neuronal isoform), in addition to eliminating the Ca^{2+}-dependent release, also increases the normally small rate of spontaneous exocytosis (8, 17).

New details on the spatial organization of Syt1 (and related C2 domain proteins) have recently emerged, which could potentially describe its dual role in orchestrating regulated exocytosis (18-21). Isolated Syt1 was discovered to polymerize into ~30 nm (diameter) sized ring-like oligomers, prompted by the binding of polyvalent anions, like ATP in solution or PS/PIP2 on membranes, to a conserved polylysine motif within the C2B domain (19-21). Moreover, the ring-shaped oligomers formed on membranes are sensitive to Ca^{2+} and rapidly disassemble at physiological Ca^{2+} concentration. This is because the same surface on the C2B domain that is used to form the ring, binds Ca^{2+} and reorients into the lipid bilayer (19, 21). If these C2B derived Syt1 oligomers were to form at the site of docking, then they could potentially regulate the terminal phases of vesicular release (18). While there is yet no direct evidence that such ring oligomers exist *in vivo*, salient genetic and biochemical correlates provided by the oligomeric structure (19, 21) and the structural conservation of circular oligomerization among many C2 domain protein (21) strongly support the overall hypothesis.

In this report, we examine the physiological role of the Syt1 oligomers using a targeted mutation (F349A) that specifically disrupts the C2B-dependent oligomerization. We find that the destabilizing the Syt1 oligomers uncouples vesicular release from Ca^{2+}-influx in PC12 cells, even though the Ca^{2+}-sensing capacity and other molecular properties of Syt1 are unaltered. Our data suggests that the Syt1 oligomerization represent a central organizing principle for Ca^{2+}-coupled exocytosis in PC12 cells and may very well represent a universal mechanism underlying Ca^{2+}-regulated exocytosis under diverse settings.

RESULTS

Identification of Syt1 Ring Oligomer Disrupting Mutation

To test the functional role of the Syt1 oligomers, we sought to generate targeted mutations in Syt1 that specifically disrupt its C2B dependent oligomerization. Based on fitting the X-ray crystal structure of $Syt1^{C2AB}$ (residues 143-421) into the EM density map generated from the reconstruction of the $Syt1^{C2AB}$ coated tubes (19) (See SI Appendix, Fig. S1A), we identified putative residues in the C2B domain (Val-304, Leu-307, Tyr-311, Phe-349, Leu-394) likely to be involved in mediating Syt1 ring oligomer assembly (Fig. 1A). Given the hydrophobic nature of the dimer interface (Figure 1A), we systematically assessed the effect of polar (Asn) mutation on oligomer assembly using electron microscopy (EM) analysis as described previously (19, 21). Briefly, the lipid monolayer (PC/PS at 3:2 molar ratio) formed at the air/water interface was recovered on a carbon-coated EM grid and protein solution was added to the lipid monolayer under Ca^{2+}-free conditions (1 mM EDTA) and incubated for 1 min at 37˚C. Negative stain analysis revealed that polar (Asn) mutation of two key hydrophobic residues (Leu-307 & Phe-349) has a strong effect, with near complete elimination of $Syt1^{C2AB}$ oligomeric structures (Fig. 1B & 1C). Similar mutation of other putative residues had little or no effect on the $Syt1^{C2AB}$ polymerization (Fig. 1B & 1C). In fact, replacing Leu-307 or Phe-349 with a weak hydrophobic residue, like Alanine (L307A or F349A), was sufficient to disrupt the oligomer formation (Fig. 1B, 1C). Given the conservative nature of the Ala replacement and lower probability of off-target effects, we chose these mutations for further analysis.

F349A Mutation Selectively Affects Syt1 Oligomerization

To evaluate the specificity of the identified mutations, we examined the effect of L307A ($Syt1^{L307A}$) and F349A mutation ($Syt1^{F349A}$) on distinct molecular properties of Syt1 (Fig. 2). We measured the intrinsic Ca^{2+}-affinity of the C2B domain with Microscale Thermophoresis (MST) analysis using Alexa Fluor 488-labeled Syt1 (residue 269) WT or mutant proteins (Fig. 2A). It revealed a

comparable intrinsic Ca^{2+}-affinity for $Syt1^{WT}$ (K_{Ca} = 235.3 ± 85.6 µM) and $Syt1^{F349A}$ (K_{Ca} = 226.8 ± 40.4 µM), but a weaker binding for $Syt1^{L307A}$ mutant (K_{Ca} = 922.5 ± 83.3 µM). Since Leu-307 residue locates within the Ca^{2+}-biding loops on the Syt1 C2B domain, a mutation at this site might affect the Ca^{2+}-coordination properties of the C2B domain. Thus, we chose to focus on the F349A mutation, which does not locate within any known functional surface of Syt1, for further analysis.

Lipid binding assay showed that $Syt1^{F349A}$ readily binds PS/PIP2 containing liposomes under Ca^{2+}-free conditions and to levels comparable to the wild-type ($Syt1^{WT}$) (Fig. 2B). This indicates that the electrostatic interaction between the conserved polylysine motifs on C2B and the anionic lipids, which is needed for the close docking of vesicles to the PM under both *in vitro* and *in vivo* conditions (14, 22-24), is unaltered by the F349A mutation. Stopped-flow rapid mixing analysis (Fig. 2C) using the environment-sensitive fluorescent probe NBD (7-nitrobenz-2-oxa-1,3-diazol-4-yl-ethylenediamine) attached to the membrane penetrating loop of the C2B domain (residue V304C) showed that both the $Syt1^{WT}$ and $Syt1^{F349A}$ insert very rapidly into the bilayer upon Ca^{2+}-binding, and with similar kinetics (k_{obs} = 146 ± 4.5 s^{-1} and 144 ± 3.6 s^{-1} respectively). Likewise, MST analysis using Alexa Fluor 488-labeled SNARE complex (VAMP2 residue 28) exhibited comparable binding affinity (K_{SNARE} ~ 7 µM) to both $Syt1^{WT}$ and $Syt1^{F349A}$ implying that Syt1-SNARE interaction is unchanged (Fig. 2D). So, we conclude that F349A mutation selectively impairs Syt1 oligomerization without affecting other critical molecular properties. Further underscoring its effectiveness, the F349A mutation also disrupted the ring oligomer formation of the entire cytoplasmic domain of Syt1 (residues 96-421) under physiological lipid and buffer conditions (See SI Appendix, Fig. S1B).

F349A Mutation Eliminates Ca^{2+}-control of exocytosis in PC12 cells

We assessed the effect of the F349A mutation on vesicular exocytosis using rat adrenal pheochromocytoma (PC12) cells, a widely used model system for studying neurosecretion (25, 26). Specifically, we expressed both $Syt1^{WT}$ and $Syt1^{F349A}$ in a Syt1-deficient PC12 cell line (F7-cells) (27) and performed live-cell total internal reflection fluorescence microscopy (TIRFM) imaging to monitor single exocytotic events by employing pHluorin-tagged (luminal) VAMP2 (28-31) (Fig. 3). We chose VAMP2- pHluorin as fusion reporter as it serves as a universal marker for all vesicle types (small clear vesicles; small & large dense core vesicles) in PC12 cells and in our TIRFM setup, the pHluorin signal increase corresponding to a fusion event can be automatically detected and scored by a differential analysis of the images (29-31).

Quantitative immunoblot analysis (Fig. 3A & See SI Appendix, Fig. S2) and immunofluorescence analysis (Fig. 3B) of the untransfected F7 cells (with normal PC12 cells as reference) confirmed the absence of Syt1 expression, but also revealed a significant reduction (~50%) in the expression of Syt9, a closely related isoform implicated in mediating Ca^{2+}-dependent release in PC12 cells (32). Correspondingly, untransfected F7 cells showed a significant reduction in number of fusion events as compared to the control PC12 cells. Notably, both the constitutive and Ca^{2+}-stimulated vesicle fusion was diminished (Fig. 3C), hinting at possible impairment of vesicle docking/priming process. This was confirmed by EM data showing a significant reduction of vesicle density in the immediate vicinity of the plasma membrane in the F7 cells (Fig. 3D).

Overexpression of $Syt1^{WT}$ in this background partially rescued vesicle docking (Fig. 3D) and restored the fusion properties to the control levels (Fig. 3C). Particularly, it reestablished the Ca^{2+}-control of exocytosis with a low rate of constitutive exocytotic events (~3 events per minute) as compared to robust regulated exocytosis (~10 fusion events per minute) when triggered by potassium chloride (KCl) depolarization in the presence of Ca^{2+}. This strictly required Ca^{2+}-binding to Syt1, specifically to the C2B domain, as disrupting its Ca^{2+}-binding ability using targeted mutations (D309A, D363A, D365A; $Syt1^{3A}$) completely abolished the Ca^{2+}-induced enhancement of vesicular release (Fig. 3C).

$Syt1^{F349A}$ similarly rescued the docking phenotype, with density and distribution of vesicles very similar to the $Syt1^{WT}$ (Fig. 3D). However, the number of spontaneous exocytotic events under resting conditions increased approximately ~3 fold when compared to the rescue with $Syt1^{WT}$ construct (Fig. 3C). Strikingly, $Syt1^{F349A}$ overexpression occluded the Ca^{2+}-dependent increase of vesicular exocytosis triggered by KCl depolarization (Fig. 3C). In essence, the F349A mutation eliminated the tight Ca^{2+}-regulation of vesicle fusion in PC12 cells. Disrupting the Ca^{2+}-binding to the C2B in this background ($Syt1^{3A/F349A}$) had a small overall effect on vesicular exocytosis (Fig. 3C), with near identical number of exocytotic events observed under both basal and stimulating conditions as compared to $Syt1^{F349A}$ (Fig. 3C). Nonetheless, the number of constitutive exocytotic events was still significantly higher compared to the $Syt1^{WT}$ rescue conditions (Fig. 3C). This implies that the significant portion of the exocytotic events observed with $Syt1^{F349A}$ rescue are constitutive-in-nature (i.e. Ca^{2+}-independent), even under Ca^{2+}-stimulating conditions.

To verify that the observed phenotype under $Syt1^{F349A}$ rescue condition is specifically caused by the disruption of the Syt1 oligomerization and to rule out any indirect or off-target effects, we tested and obtained similar results with two additional, independent vesicle fusion reporters - Synaptophysin-pHluorin as a marker for small, clear vesicle and NPY-pHluorin as a dense-core

vesicle maker. (See SI Appendix, Fig. S3). Additionally, we confirmed that expression levels of other PC12-associated Syt isoforms (Syt4, Syt7, Syt9) and the SNARE proteins, Syntaxin1 and SNAP25 (Fig. 3A & See SI Appendix, Fig. S2) were unaltered by Syt1^{F349A} over-expression. Viewed together, these data strongly support the model that the C2B-dependent oligomerization of Syt1 suppress spontaneous fusion events to enable Ca^{2+}-regulated vesicle exocytosis in PC12 cells. It further argues that the Ca^{2+}-dependent step of regulated exocytosis might primarily involve removing this inhibition on fusion machinery as opposed to direct activation of membrane fusion.

DISCUSSION

The data presented here establish Syt1 oligomerization as a critical component of Ca^{2+}-coupling mechanism. This follows from rescue experiments in Syt1-deficient PC12 cells (F7 cells) showing that disrupting the Syt1 oligomerization results in abolition of Ca^{2+}-control of exocytosis. In our pHluorin-based optical assay, we observe a significant reduction in overall exocytosis in the untransfected F7 cell-line (Fig. 3C). However, earlier studies employing bulk secretion assays, have reported little or no defect in Ca^{2+}-triggered exocytosis using the same cell line (27, 32). Under those conditions, increased expression of a closely related Synaptotagmin isoform, Syt9 compensates for Syt1 deficiency and indeed Syt1/Syt9 double deficiency results in complete loss of exocytosis (32, 33). In our untransfected F7 cell-line, we observe a significant reduction (~50%) in the Syt9 expression levels in addition to Syt1 deficiency (Fig. 3A). Since the F7 cell line dates back ~25 years, genotypic and phenotypic variation could have occurred over an extended period of time (34-36). We believe that the combination of Syt1 deficiency and reduced Syt9 expression in our F7 cell-line likely explains the strong loss-of-exocytosis phenotype observed (Fig. 3C). Consistent with the fusion phenotype, we also observe clear deficiency in docking of the dense core vesicles in the untransfected F7 cells (Fig. 3D). It is worth noting that in our experimental conditions overexpression of Syt1^{WT} was able to partially rescue the docking phenotype and fully restore the fusion properties, including the Ca^{2+}-regulated exocytosis, to the control PC12 cell levels (Fig. 3). This provides an ideal background to relate the effect of disrupting the oligomer formation using the Syt1^{F349A} mutant.

We further note that the observed effect of the Syt1 deficiency appears to be highly dependent on the choice of the reporter. Syt1 deficiency has been shown to: increase the release of dopamine/ATP (27), have no effect or drastically reduce the release of norepinephrine (32), reduce the release of catecholamines, and abolish NPY release (37, 38). In the current study, we use VAMP2-pHluorin, a universal reporter for exocytosis from all types of vesicles in PC12 cells. We additionally confirmed our fusion phenotype for untransfected and for both WT and F349A

rescue conditions using independent reporters, Synaptophysin-pHluorin and NPY-pHluorin specific for small, clear vesicles and dense core vesicles, respectively (See SI Appendix, Fig. S3).

How does the Syt1 oligomerization reversibly clamp fusion? We envision a concerted mechanism wherein the full complement (15-20 copies) of Syt1 on the vesicle oligomerize at the site of docking triggered by PIP2 binding (Fig. 4). It is then ideally positioned to simultaneously template multiple SNAREpins, likely using the recently identified 'primary' binding site involving SNAP25 and C2B domain (9, 18), which is accessible and free to interact in the ring oligomer (21). The height of Syt1 oligomers combined with the SNAREs atop would maintain the two bilayers far apart (~4 nm) to allow the N-terminal assembly but sterically block the complete assembly (18). The SNAREpin bound to the Syt1 ring oligomer would also be restrained from moving radially inwards in the membrane plane, preventing full-zippering (18). In this manner, the Syt1 oligomerization lowers the probability of the fusion of the docked vesicle in the absence of the Ca^{2+}-trigger (Fig. 4).

It is possible that the C2B oligomers dynamically break and re-form, and intact ring-like oligomers observed *in vitro* are not always present or predominate *in vivo*. Under these conditions, very short oligomers of Syt1 could serve to clamp SNAREpins by restraining them from rotating away from the ideal orientation in which C-terminal zippering is sterically prevented. However, such a stochastic mechanism would produce an inefficient clamp as the SNAREpin can 'twist' out position and complete zippering, leading to fusion (18). Thus, we favor a more concerted mechanism, in which in the Syt1 ring-like oligomers acts as a 'primer' to template and link multiple SNARE proteins, and along with the SNARE-associated chaperones (Munc13 & Munc18) and regulators (Complexin) enable rapid, Ca^{2+}-coupled vesicular release (18). Additionally, this arrangement would allow for binding of other Syt isoforms to the templated SNARE proteins via the conserved Complexin-dependent 'tripartite' binding site (10) and, thus provides a plausible framework to describe the synergistic action of different Syt isoforms (39). While precise molecular architecture of the clamped state is still unclear, the Syt1 oligomer-based model provides the most elegant solution of a symmetrical structure that balances the physical forces to maximize stability prior to release (18).

The Syt1 oligomers are disassembled upon Ca^{2+}-influx which liberates the partially assembled SNAREpins to complete zippering and open the fusion pore cooperatively (Fig. 4). Syt1 oligomerization, by the virtue of stabilizing the Ca^{2+}-binding loops at the dimer interface (20, 21), would also prevent any extemporary membrane insertion (40) and thus, ensure vesicular release only when the critical intracellular [Ca^{2+}] is reached. Thus, the Syt1 oligomerization synchronizes

vesicle fusion to Ca^{2+}-influx. Additionally, our data suggests that the Ca^{2+}-triggered loop insertion of the Syt1 principally serves to reverse the 'clamp' on the fusion machinery and any additional contribution in promoting membrane fusion by lipid bilayer perturbations (41) plays an auxiliary role. This is an emerging and speculative concept (18, 42) and requires further research.

While the clustering of synaptotagmin at nerve terminals has been reported (43), the oligomeric structures (intact or dynamic) that we propose have not been directly observed. We note that the methods applied to date under both *in vivo* and *in vitro*, would not be expected to reveal these structures without intentional effort, in particular to preserve these metastable structures. Thereby, focused high-resolution structural studies within the cellular context will be needed to confirm the general outline of this model and to provide intimate details. Nevertheless, given C2-domain oligomerization is a conserved feature among C2-domain proteins (21), many of which regulate exocytosis, we believe that diverse forms of intercellular communications and physiological response may also rely on similar clamping and triggering mechanism to govern the fusion machinery.

EXPERIMENTAL PROCEDURES

Materials. The following DNA constructs, which have been previously generated and sequenced (13, 19, 21, 44), were used: pCDFDuet-GST-Precission-Syt1^{C2AB} (rat Synaptotagmin-1 residues 143-421); pGEX GST-Thrombin-Syt1^{CD} (rat Synaptotagmin-1 residues 96-421) wild type and single cysteine mutants at residue 269 (E269C) and residue 304 (V304C); pET28a oligohistidine-Thrombin-syntaxin1A (rat Syntaxin1a residues 191-253), pET28a oligohistidine-SUMO-SNAP25A (residues 1-203); pET15b-oligohistidine-Thrombin-VAMP2 (human VAMP2 residues 1-96) with a single cysteine at residue 28 (S28C). In addition, the following Syt1 mutants were created in this study: V304N, L307N, L307A, Y311N, F349N, F349A and L394N in the Syt1^{C2AB} background and F349A in Syt1^{CD} background using the QuickChange mutagenesis kit (Agilent Technologies, Santa Clara, CA). All recombinant proteins were expressed and purified as described previously (13, 19, 21, 44). The VAMP2-pHluorin construct used has been described previously (28). For generation of the HA-tagged Syt1 plasmids used for transfections of F7 cells, the full-length rat Syt1 cDNA was cloned into a pCMV-HA-N vector (Clontech, Mountain View, CA) that had been modified by inserting a 25 amino acid signal sequence of preprotachykinin upstream of the HA tag using the ApaI restriction site. The NPY-pHluorin construct was generated by amplifying human NPY from NPY-mCherry (Addgene Cat #67156) and inserting into the pCIneo vector (Promega) with a 6 amino acid linker upstream of a pHluorin tag. The pcDNA3 rat Synaptophysin-pHluorin construct was obtained from Addgene Inc. (Cat #37003). PC12 cell line

was a gift from Dr. Barbara Ehrlich, Yale University and the Syt1-deficient PC12 termed F7 cells were purchased from RIKEN BRC (Cat# RCB2800, RRID: CVCL_T752). Lipids 1-palmitoyl-2-oleoyl-sn-glycero-3-phosphocholine (POPC), 1,2-dioleoyl-sn-glycero-3-phospho-L-serine (DOPS) and phosphatidylinositol 4, 5-bisphosphate (PIP2) were purchased from Avanti Polar lipids (Alabaster, AL). Thiol reactive fluorescent probes Alexa488-maleimide and IANBD Amide (N,N'-Dimethyl-N-(Iodoacetyl)-N'-(7-Nitrobenz-2-Oxa-1,3-Diazol-4-yl)Ethylenediamine) were purchased from Thermo Scientific, Waltham, MA.

Lipid Monolayer Assay. The monolayers were setup as described previously (19, 21). Briefly, degassed ultrapure H_2O was injected through a side port to fill up wells (4 mm diameter, 5 mm depth) in a Teflon block. The flat-water surface was coated with 0.6 µl of phospholipid mixture. The following lipid mixtures were used: PC/PS with molar ratio of 60:40 (for $Syt1^{C2AB}$ experiments), or PC/PS/PIP2 with molar ratio of 72.5:25:2.5 (for $Syt1^{CD}$ experiments), which were pre-mixed as required, dried under N2 gas and then re-suspended in chloroform to a final total lipid concentration of 0.5 mM. The Teflon block then was stored in a sealed humidity chamber for 1h at room temperature to allow the chloroform to evaporate. Continuous carbon-coated EM grids were baked at 70 °C for 4 h and washed with hexane to improve hydrophobicity. Lipid monolayers formed at the air/water interface were then recovered by placing the pre-treated EM grid (400 mesh; Ted Pella) carbon side down on top of each water droplet for 1 min. The grid was raised above the surface of the Teflon block by injecting ultrapure H_2O into the side port and then was lifted off the droplet immediately.

Proteins were rapidly diluted to 3 µM in 20 mM MOPS, pH 7.5, 15 mM KCl, 1 mM EDTA, 2 mM $MgAC_2$, 1 mM DTT, 5% (wt/vol) trehalose buffer and then added to the lipid monolayer on the grid and incubated in a 37°C humidity chamber for 1 min. The final KCl concentration in the buffer was adjusted to 100 mM as required. To facilitate structural analysis of the ring-like structrures, we further optimized the incubation conditions by using an annealing procedure: rings were nucleated at 37°C for 1 min followed by a 30-min annealing step at 4 °C. The grids were rinsed briefly (~10 s) with incubation buffer alone or with buffer supplemented with $CaCl_2$ (0.1, 0.5 and 1 mM free) for Ca2+ treatment studies. The free [Ca2+] was calculated by Maxchelator (maxchelator.stanford. edu). Subsequently, the grids were blotted with Whatman#1 filter paper, negatively stained with uranyl acetate solution (1% wt/vol), and air dried. The negatively stained specimens were examined on a FEI Tecani T12 operated at 120 kV. The defocus range used for our data was 0.6–2.0 µm. Images were recorded under low-dose conditions (~20 $e^-/Å^2$) on a 4K × 4K CCD camera (UltraScan 4000; Gatan, Inc.), at a nominal magnification of 42,000×.

Micrographs were binned by a factor of 2 at a final sampling of 5.6 Å per pixel on the object scale. The image analysis, including size distribution measurements, was carried out using Image J software.

Liposome Flotation Assay. Ca^{2+}-independent Syt1-membrane interaction was measured using a liposome floatation assay as described previously (21). $Syt1^{CD}$ (WT & F349A) were incubated with PS/PIP2 liposomes (71.5% PC, 25% PS, 2.5% PIP2,1% NBD) for 1h at room temperature and separated using a discontinuous Nycodenz (Sigma-Aldrich, St. Louis, MO) gradient. The bound fraction (normalized to the lipid using NBD-fluorescence) was then estimated using densitometry analysis of SDS-PAGE gels using Image J software(45).

Microscale Thermophoresis Analysis. $Syt1^{WT}$, $Syt1^{F349A}$ and $Syt1^{L307A}$ interaction with Ca^{2+} and the SNARE complex were quantified using Microscale Themrophoresis (NanoTemper, Munich, Germany) as described previously (46). For Ca^{2+}-binding analysis, MST was measured with ~ 50 nM of $Syt1^{CD}$ (WT, L307A and F349A) labeled with Alexa488 at residue 269 (E269C) in 25 mM HEPES, 100 mM KCl, 2.5 mg/ml BSA, 0.5% tween, and pH 7.4 using premium coated capillaries. Similar conditions and setup were used to measure Syt1-SNARE interaction, but using ~10 nM of Alexa488 labeled pre-assembled SNARE complex (VAMP2 residue 28) and unlabeled Syt1 (WT & F349A). The MST curves were fitted with simple Michaelis-Menten kinetics to obtain the apparent dissociation constant for Ca^{2+} and SNARE binding. Note: For the Syt1-SNARE interaction studies, MST data beyond 50 µM Syt1 concentration were not included in the analysis due to precipitation of Syt1 protein at high concentration under these experimental conditions.

Stopped-flow Rapid Mixing Analysis. To monitor Ca^{2+}-triggered membrane interaction of the Syt1 (WT & F349A), the tips of the Ca^{2+} binding loops of the C2B domain ($Syt1^{CD}$ residue 304) were labeled with an environment-sensitive probe, NBD. Stopped-flow rapid mixing analysis was carried out using Applied Photophysics SX20 instrument (Applied Photophysics Ltd, Surrey, UK) as described previously (13) with the fluorescently labeled Syt1 pre-incubated with PS/PIP2 liposome (72% PC, 25% PS, 3% PIP2) loaded in one syringe and buffer containing EGTA or Ca^{2+} in the other syringe. The samples were mixed rapidly (dead time ~ 1 msec) yielding a final concentration of 0.2 mM EGTA and 1mM Ca^{2+}. The change in fluorescence signal collected with a 510 nm cutoff filter (Ex 460 nm) was fitted with a single exponential function to calculate the observed rate of insertion of the Ca^{2+}-loops.

Live Cell Imaging. PC12 cells and the Syt1 deficient F7 cells (27) were incubated at 37°C in 5% CO_2 in DMEM, supplemented with 10% Horse Serum, 5% FBS, MEM Non-Essential Amino Acid,

1mM Sodium Pyruvate and 100 µg/mL penicillin/streptomycin (Gibco, Gaithersburg, MD). F7 cells were cultured in tissue culture flasks pre-treated with fibronectin or collagen-4 as they were not as adherent as the wild-type PC12 cells. F7 cells were electroporated using the Amaxa Nucleofector method (VVCA-1003KT, Lonza) with ~1-1.5 µg of Vamp2-pHluorin plasmid DNA and ~1-1.5 µg of either $Syt1^{WT}$ or $Syt1^{F349A}$ plasmid DNA, with a typical transfection efficiency ~60%. Protein expression was verified by Western Blot analysis using a mouse anti-Syt1 antibody (Synaptic Systems, Göttingen, Germany). For imaging, cells were plated on 35-mm tissue culture dishes with cover glass bottom (refractive index, 1.51; World Precision Instruments, Sarasota, FL), precoated with poly-D-lysine and fibronectin; and imaged 48h later. Medium was replaced with Live Cell Imaging Solution (Thermo Fisher Scientific, Waltham, MA) supplemented with 1.3 mM Ca^{2+} and cells were imaged at 37°C using a custom made TIRFM (30, 31, 47, 48) set up based on an Olympus IX-70 inverted microscope fitted with a 60x 1.45 N.A. TIRFM lens (Olympus, Melville, NY) and controlled by µManager software (http://www.micro-manager.org). pHluorin was excited by the 488 nm line of an Innova 70C-Spectrum ion laser (Coherent, Santa Clara, CA). Cells were imaged at 6.6 Hz with 150 ms exposure using a Zyla 4.2 Megapixel Camera (Andor Technologies). The emission was collected through a BrightLine® full-multiband laser filter set, optimized for 405, 488, 561, & 635 nm laser sources (Semrock, part number LF405/488/561/635-A-000). PC12 cells were stimulated for exocytosis in the Live Cell Imaging Solution (Thermo Fisher Scientific, Waltham. MA). The tip of a micropipette containing a stimulating solution (Live Cell Imaging Solution with 1.3 mM $CaCl_2$ and 100 mM KCl) was positioned near the target cell with a micromanipulator (Warner Instruments, Hamden, CT). The stimulating solution was pressure ejected with picospritzer II (Parker Instrumentation, General Valve Division, Fairfield, NJ). Single-vesicle exocytosis events were automatically detected using a Matlab software described previously (30, 31, 47, 48). The statistical significance of the fusion results was established using a Wilcoxon-Mann-Whitney to account for the non-normal distribution of the data using the open source software Gnumeric (www.gnumeric.org).

Immunoblot analysis. Cells (cultured PC12, F7 cells and F7 cells transfected with either $Syt1^{WT}$ or $Syt1^{F349A}$) were grown in six-well plates. After 48h, cells were washed, detached, and collected by centrifugation. Pellets were re-suspended in radio-immunoprecipitation assay (RIPA) buffer for 3-5 h followed by spin down at top speed (20,817g) in a bench-top centrifuge for 30 min. Protein estimation in the post-nuclear cell lysates was performed using Bicinchoninic acid (BCA) assay reagent from Pierce (Rockford, IL). Equal quantity (~15-20 µg) of protein from four cell lysates were first separated in SDS-PAGE and then transferred onto PVDF membranes (Millipore, Billerica, MA) for immune-blotting. After being blocked with Odyssey Blocking Buffer (LI-COR

Biosciences, Lincoln, NE, USA), the membranes were incubated with appropriate primary antibodies. The following primary antibodies from Synaptic Systems (Göttingen, Germany) were used: Syt1 (cat# 105011), Syt9 (cat# 105053) Syt4 (cat# 105043), Syt7 (cat# 105173), SNAP25 (cat# 111011) and Syntaxin1 (cat # 110011). The levels of individual proteins were determined by quantitative Western blots with IRDye conjugated secondary antibodies (IRDye® 680RD Goat anti-Mouse IgG or IRDye® 680RD Goat anti-Rabbit IgG) on a LI-COR infrared imaging system. Fluorographs were quantitatively scanned using ImageStudio.

Immunofluorescence. Cells (cultured PC12, syt-1 deficient F7 cells and F7 cells transfected with $Syt1^{WT}$ or $Syt1^{F349A}$) on coverslips, pre-treated with poly-D-lysine and fibronectin, were fixed and prepared for immunofluorescence against Syt1 (mouse Syt1 antibody tagged with Oyster 550 (Synaptic Systems, Gottingen, Germany) was used.

Electron microscopy Analysis. Cultured PC12, Syt-1 deficient F7 cells and F7 cells transfected with either syt-1-wt or syt-1-F349A on coverslips, pretreated with poly-D-lysine and fibronectin, were fixed in 2.5% glutaraldehyde in 0.1 M sodium cacodylate buffer (pH 7.4) at room temperature for 1 h. The cells were then rinsed twice in the same buffer and post-fixed in 0.5% osmium tetroxide (OsO_4) at room temperature for 30 min, followed by another 30 min in 1% tannic acid solution. Specimens were stained *en bloc* with 2% aqueous uranyl acetate for 15 min, dehydrated in a graded series of ethanol to 100% and embedded in Polybed 812 resin. Blocks were polymerized in 60˚C oven for 24 h. Thin sections (60 nm) were cut by a Leica ultramicrotome and post-stained with 2% uranyl acetate and lead citrate. Cell sections were examined with a FEI Tecnai transmission electron microscope at 80 kV accelerating voltage; digital images were recorded with an Olympus Morada CCD camera and iTEM imaging software. ImageJ software(45) was used to measure the distance of each individual dense core vesicle from the closest plasma membrane (outer membrane – outer membrane distance). An average of 10-15 cells per condition with a minimum of ~500 vesicle was used to create the cumulative distribution plot.

ACKNOWLEDGEMENTS

We thank the National Institute of Health (NIH) grant DK027044 to JER for support of this research. This work was also supported by the Wellcome Trust Strategic Award (Reference: 104033) to JER & KV. We wish to thank Dr. Xinran Liu and Morven Graham at CCMI EM Core Facility, Yale School of Medicine for technical inputs and support.

REFERENCES

1. Burgess TL & Kelly RB (1987) Constitutive and regulated secretion of proteins. *Annu Rev Cell Biol* 3:243-293.
2. Gerber SH & Sudhof TC (2002) Molecular determinants of regulated exocytosis. *Diabetes* 51 Suppl 1:S3-11.
3. Sudhof TC (2013) Neurotransmitter release: the last millisecond in the life of a synaptic vesicle. *Neuron* 80(3):675-690.
4. Sollner T*, et al.* (1993) SNAP receptors implicated in vesicle targeting and fusion. *Nature* 362(6418):318-324.
5. Weber T*, et al.* (1998) SNAREpins: minimal machinery for membrane fusion. *Cell* 92(6):759-772.
6. Brose N, Petrenko AG, Sudhof TC, & Jahn R (1992) Synaptotagmin: a calcium sensor on the synaptic vesicle surface. *Science* 256(5059):1021-1025.
7. Fernandez-Chacon R*, et al.* (2001) Synaptotagmin I functions as a calcium regulator of release probability. *Nature* 410(6824):41-49.
8. Geppert M*, et al.* (1994) Synaptotagmin I: a major Ca2+ sensor for transmitter release at a central synapse. *Cell* 79(4):717-727.
9. Zhou Q*, et al.* (2015) Architecture of the synaptotagmin-SNARE machinery for neuronal exocytosis. *Nature* 525(7567):62-67.
10. Zhou Q*, et al.* (2017) The primed SNARE-complexin-synaptotagmin complex for neuronal exocytosis. *Nature* 548(7668):420-425.
11. Rhee JS*, et al.* (2005) Augmenting neurotransmitter release by enhancing the apparent Ca2+ affinity of synaptotagmin 1. *Proc Natl Acad Sci U S A* 102(51):18664-18669.
12. Paddock BE*, et al.* (2011) Membrane penetration by synaptotagmin is required for coupling calcium binding to vesicle fusion in vivo. *J Neurosci* 31(6):2248-2257.
13. Krishnakumar SS*, et al.* (2013) Conformational dynamics of calcium-triggered activation of fusion by synaptotagmin. *Biophys J* 105(11):2507-2516.
14. Bai J, Tucker WC, & Chapman ER (2004) PIP2 increases the speed of response of synaptotagmin and steers its membrane-penetration activity toward the plasma membrane. *Nat Struct Mol Biol* 11(1):36-44.
15. Bai J, Wang P, & Chapman ER (2002) C2A activates a cryptic Ca(2+)-triggered membrane penetration activity within the C2B domain of synaptotagmin I. *Proc Natl Acad Sci U S A* 99(3):1665-1670.
16. Paddock BE, Striegel AR, Hui E, Chapman ER, & Reist NE (2008) Ca2+-dependent, phospholipid-binding residues of synaptotagmin are critical for excitation-secretion coupling in vivo. *J Neurosci* 28(30):7458-7466.
17. Bacaj T*, et al.* (2013) Synaptotagmin-1 and synaptotagmin-7 trigger synchronous and asynchronous phases of neurotransmitter release. *Neuron* 80(4):947-959.
18. Rothman JE, Krishnakumar SS, Grushin K, & Pincet F (2017) Hypothesis - buttressed rings assemble, clamp, and release SNAREpins for synaptic transmission. *FEBS Lett* 591(21):3459-3480.
19. Wang J*, et al.* (2014) Calcium sensitive ring-like oligomers formed by synaptotagmin. *Proc Natl Acad Sci U S A* 111(38):13966-13971.

20. Wang J*, et al.* (2017) Circular oligomerization is an intrinsic property of synaptotagmin. *Elife* 6.
21. Zanetti MN*, et al.* (2016) Ring-like oligomers of Synaptotagmins and related C2 domain proteins. *Elife* 5.
22. Parisotto D, Malsam J, Scheutzow A, Krause JM, & Sollner TH (2012) SNAREpin assembly by Munc18-1 requires previous vesicle docking by synaptotagmin 1. *J Biol Chem* 287(37):31041-31049.
23. Loewen CA, Lee SM, Shin YK, & Reist NE (2006) C2B polylysine motif of synaptotagmin facilitates a Ca2+-independent stage of synaptic vesicle priming in vivo. *Mol Biol Cell* 17(12):5211-5226.
24. Honigmann A*, et al.* (2013) Phosphatidylinositol 4,5-bisphosphate clusters act as molecular beacons for vesicle recruitment. *Nat Struct Mol Biol* 20(6):679-686.
25. Burgoyne RD & Morgan A (1998) Analysis of regulated exocytosis in adrenal chromaffin cells: insights into NSF/SNAP/SNARE function. *Bioessays* 20(4):328-335.
26. Westerink RH & Ewing AG (2008) The PC12 cell as model for neurosecretion. *Acta Physiol (Oxf)* 192(2):273-285.
27. Shoji-Kasai Y*, et al.* (1992) Neurotransmitter release from synaptotagmin-deficient clonal variants of PC12 cells. *Science* 256(5065):1821-1823.
28. Miesenbock G, De Angelis DA, & Rothman JE (1998) Visualizing secretion and synaptic transmission with pH-sensitive green fluorescent proteins. *Nature* 394(6689):192-195.
29. Coleman J*, et al.* (2018) PRRT2 Regulates Synaptic Fusion by Directly Modulating SNARE Complex Assembly. *Cell Rep* 22(3):820-831.
30. Sebastian R*, et al.* (2006) Spatio-temporal analysis of constitutive exocytosis in epithelial cells. *IEEE/ACM Trans Comput Biol Bioinform* 3(1):17-32.
31. Toomre D (2012) Generating live cell data using total internal reflection fluorescence microscopy. *Cold Spring Harb Protoc* 2012(4):439-446.
32. Fukuda M, Kowalchyk JA, Zhang X, Martin TF, & Mikoshiba K (2002) Synaptotagmin IX regulates Ca2+-dependent secretion in PC12 cells. *J Biol Chem* 277(7):4601-4604.
33. Lynch KL & Martin TF (2007) Synaptotagmins I and IX function redundantly in regulated exocytosis but not endocytosis in PC12 cells. *J Cell Sci* 120(Pt 4):617-627.
34. Geraghty RJ*, et al.* (2014) Guidelines for the use of cell lines in biomedical research. *Br J Cancer* 111(6):1021-1046.
35. Lorsch JR, Collins FS, & Lippincott-Schwartz J (2014) Cell Biology. Fixing problems with cell lines. *Science* 346(6216):1452-1453.
36. Sato S, Rancourt A, Sato Y, & Satoh MS (2016) Single-cell lineage tracking analysis reveals that an established cell line comprises putative cancer stem cells and their heterogeneous progeny. *Sci Rep* 6:23328.
37. Moore JM, Papke JB, Cahill AL, & Harkins AB (2006) Stable gene silencing of synaptotagmin I in rat PC12 cells inhibits Ca2+-evoked release of catecholamine. *Am J Physiol Cell Physiol* 291(2):C270-281.
38. Roden WH*, et al.* (2007) Stable RNA interference of synaptotagmin I in PC12 cells results in differential regulation of transmitter release. *Am J Physiol Cell Physiol* 293(6):C1742-1752.

39. Volynski KE & Krishnakumar SS (2018) Synergestic control of neurotransmitter release by different members of the synaptotagmin family. *Curr Opin Neurobiol*.
40. Gruget C*, et al.* (2018) Rearrangements under confinement lead to increased binding energy of Synaptotagmin-1 with anionic membranes in Mg(2+) and Ca(2). *FEBS Lett* 592(9):1497-1506.
41. Martens S, Kozlov MM, & McMahon HT (2007) How synaptotagmin promotes membrane fusion. *Science* 316(5828):1205-1208.
42. Brunger AT, Leitz J, Zhou Q, Choi UB, & Lai Y (2018) Ca(2+)-Triggered Synaptic Vesicle Fusion Initiated by Release of Inhibition. *Trends Cell Biol*.
43. Willig KI, Rizzoli SO, Westphal V, Jahn R, & Hell SW (2006) STED microscopy reveals that synaptotagmin remains clustered after synaptic vesicle exocytosis. *Nature* 440(7086):935-939.
44. Krishnakumar SS*, et al.* (2011) A conformational switch in complexin is required for synaptotagmin to trigger synaptic fusion. *Nat Struct Mol Biol* 18(8):934-940.
45. Schneider CA, Rasband WS, & Eliceiri KW (2012) NIH Image to ImageJ: 25 years of image analysis. *Nat Methods* 9(7):671-675.
46. van den Bogaart G, Meyenberg K, Diederichsen U, & Jahn R (2012) Phosphatidylinositol 4,5-bisphosphate increases Ca2+ affinity of synaptotagmin-1 by 40-fold. *J Biol Chem* 287(20):16447-16453.
47. Xu Y*, et al.* (2011) Dual-mode of insulin action controls GLUT4 vesicle exocytosis. *J Cell Biol* 193(4):643-653.
48. Rivera-Molina F & Toomre D (2013) Live-cell imaging of exocyst links its spatiotemporal dynamics to various stages of vesicle fusion. *J Cell Biol* 201(5):673-680.

.

FIGURE LEGEND

Figure 1. Identification of Synaptotagmin1 Ring Oligomer Disrupting Mutation. (A) Reconstruction of the Syt1 ring-like oligomer (19) shows that the interaction of the C2B domain (grey) drives the oligomerization with the Ca^{2+}-loops (yellow) locating to the dimer interface, while the C2A domain (cyan) appends the C2B ring oligomer. (B & C) Mutational analysis of the key hydrophobic residues locating to the oligomeric interface showing alteration of Leu-307 (magenta) and Phe-349 residue (red) significantly reduces the number of oligomers formed with the minimal C2AB domain ($Syt1^{C2AB}$) on lipid monolayer (60:40 PC/PS) as visualized by negative stain electron microscopy analysis. Mutation of other putative residues, Val-304 (green), Tyr-311 (blue) or Leu-394 (orange) showed no effect on the $Syt1^{C2AB}$ polymerization. Representative micrographs are shown and average and deviations from three independent experiments are included.

Figure 2. The F349A mutation selectively disrupts the Synaptotagmin 1 oligomerization. (A) Ca^{2+} binding measured by MST analysis using Alexa Fluor 488-labeled (residue 269) Syt1 shows that L307A mutation (blue) lowers the intrinsic Ca^{2+}-affinity, but the F349A mutation (red) has no effect as compared to WT (black). The F349A mutation also does not affect other molecular properties, namely (B) the Ca^{2+}-independent lipid binding examined by liposome floatation analysis; (C) Ca^{2+}-triggered membrane interaction of the C2B domain tracked by stopped-flow rapid mixing analysis with the environment-sensitive fluorescent probe NBD (7-nitrobenz-2-oxa-1,3-diazol-4-yl-ethylenediamine) attached to the C2B domain residue V304C and (D) ability to bind SNARE complex assessed by MST analysis using Alexa Fluor 488-labeled SNARE complex (VAMP2 residue 28) . Representative gel & curves are shown and the average and deviation from three independent experiments are included. K_{Ca}: Ca^{2+}-binding constant; K_{obs}: observed rate of loop insertion, K_{SNARE}: SNARE binding constant.

Figure 3. Disrupting the Syt1 oligomerization occludes Ca^{2+}-control of exocytosis in PC12 cells. (A) Representative Western Blot showing that untransfected F7 cells lack Syt1 expression, but exhibit reduced expression of Syt9, a closely related isoform. It further shows the rescue of Syt1 expression in the F7 cells with $Syt1^{WT}$ or $Syt1^{F349A}$ leads to no alteration in the expression of other Syt isoforms and the SNARE proteins (See SI Appendix, Fig S2 for quantitative analysis). (B) Representative immunofluorescence analysis using anti-Syt1 antibody shows a similar distribution of the endogenous Syt1 in PC12 cells and the recombinant $Syt1^{WT}$ or $Syt1F^{349A}$ expressed in F7 cells (C) Effect of $Syt1^{349A}$ mutation on exocytosis assessed by VAMP2-pHluorin TIRFM imaging of single vesicle fusion events under basal (constitutive) and after KCl-induced

depolarization (Ca^{2+}-stimulated) conditions. Disrupting the Syt1 oligomer dysregulated exocytosis, dramatically increasing (~3-fold) the typically low levels of constitutive exocytosis, effectively abolishing the Ca^{2+}-control of exocytosis. The majority of the exocytotic events with Syt1F^{349A} rescue are constitutive-in-nature as disrupting Ca^{2+}-binding (Syt1$^{3A/F349A}$) shows little or no effect under either basal or stimulated conditions. ***P < 0.005 Wilcoxon-Mann-Whitney. (D) Electron microscopy of serial sections was used to characterize the distribution and docking of the dense core vesicles (DCV). Left, a representative micrograph of untransfected (top) or Syt1^{F349A} (bottom) expressing F7 cells. The DCV are marked by red arrows. Right, cumulative probability plots of DCV distribution relative to the plasma membrane. Untransfected F7 cells (red) showed a pronounced right shift in the distribution with fewer vesicles locating near to the PM (***P < 0.001 vs. PC12 cells, Kolmogorov–Smirnov test). This impairment in vesicle docking is partially rescued by the expression of either the Syt1^{WT} or Syt1^{F349A} (blue & green respectively). Data from N = 14 - 32 cells for each condition, with 55 ± 38 vesicles per cell (mean ± SD) from 3 independent preparations.

Figure 4. Model for Ca^{2+}-regulated exocytosis. Oligomerization of the Syt1 regulates SNARE assembly at the site of docking, specifically, it prevents the terminal zippering by sterically blocking the close approach of the vesicle and by radially restricting the assembly process. This serves to reversibly ‘clamp’ SNAREpins, until dissociated by Ca^{2+} binding. In this manner, the Syt1 oligomerization imposes Ca^{2+}-control on vesicle fusion. Disrupting the oligomerization (F349A mutation) does not affect the vesicle docking, but removes the ‘clamp’ to enhance the spontaneous fusion events and effectively abolishing Ca^{2+}-control, even though the Ca^{2+} activation mechanism is intact.

FIGURE 1

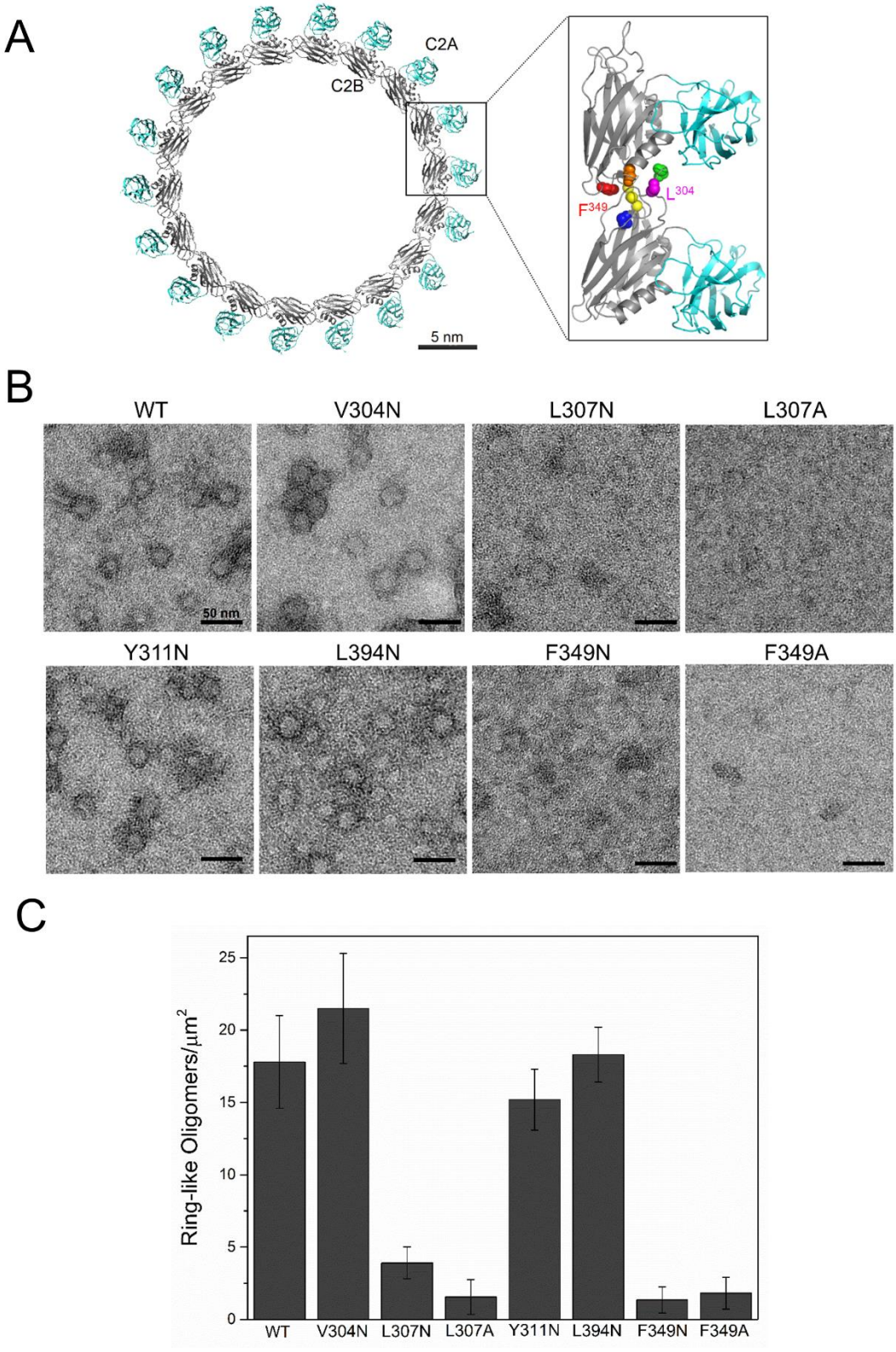
A
C2A
C2B
5 nm
F349
L304
B
WT
V304N
L307N
L307A
50 nm
Y311N
L394N
F349N
F349A
C
Ring-like Oligomers/μm2
0
5
10
15
20
25
WT
V304N
L307N
L307A
Y311N
L394N
F349N
F349A

FIGURE 2

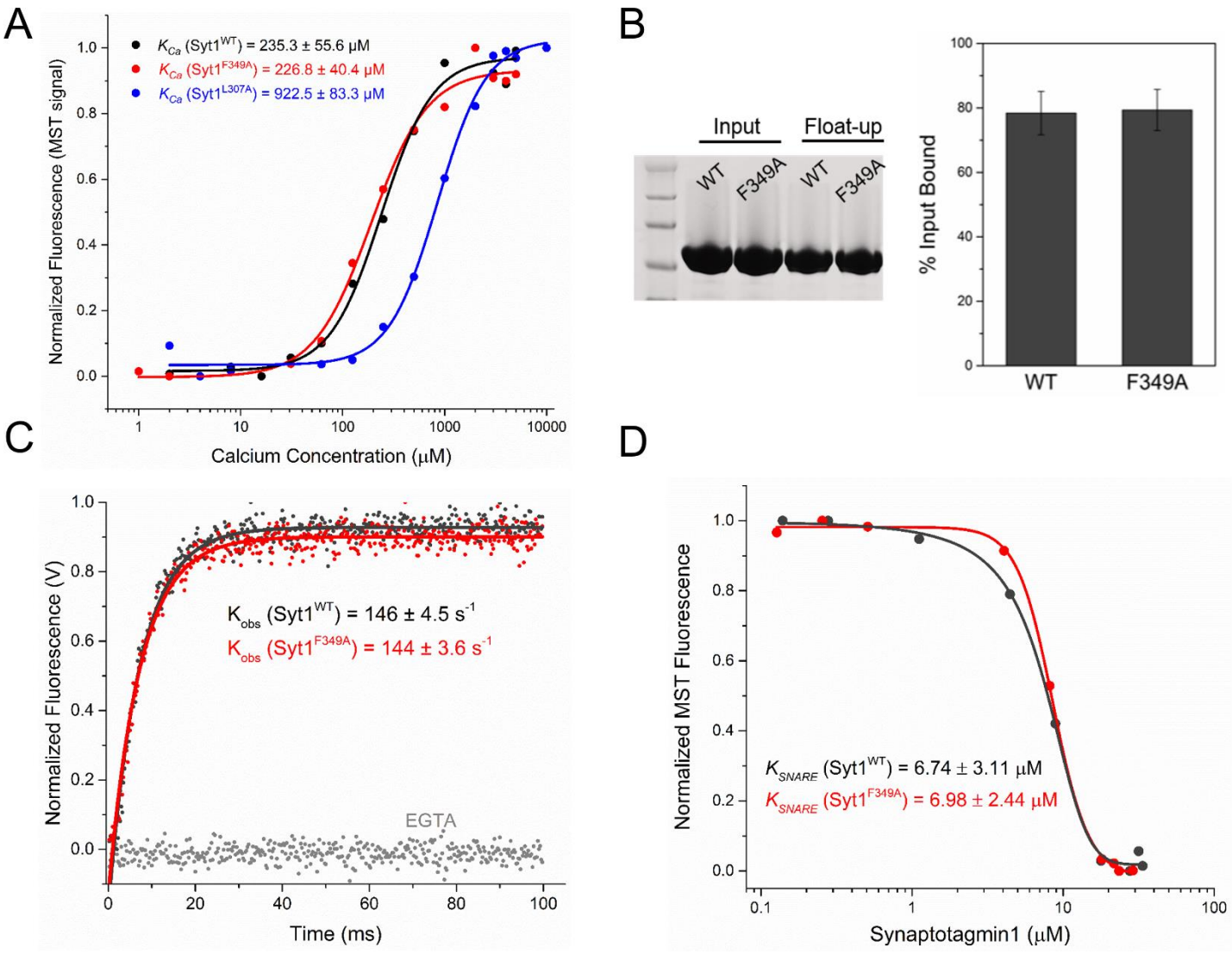
A
K_{Ca} (Syt1^{WT}) = 235.3 ± 55.6 μM
K_{Ca} (Syt1^{F349A}) = 226.8 ± 40.4 μM
K_{Ca} (Syt1^{L307A}) = 922.5 ± 83.3 μM
Normalized Fluorescence (MST signal)
Calcium Concentration (μM)
B
Input
Float-up
WT
F349A
WT
F349A
% Input Bound
WT
F349A
C
K_{obs} (Syt1^{WT}) = 146 ± 4.5 s^{-1}
K_{obs} (Syt1^{F349A}) = 144 ± 3.6 s^{-1}
EGTA
Normalized Fluorescence (V)
Time (ms)
D
K_{SNARE} (Syt1^{WT}) = 6.74 ± 3.11 μM
K_{SNARE} (Syt1^{F349A}) = 6.98 ± 2.44 μM
Normalized MST Fluorescence
Synaptotagmin1 (μM)

FIGURE 3

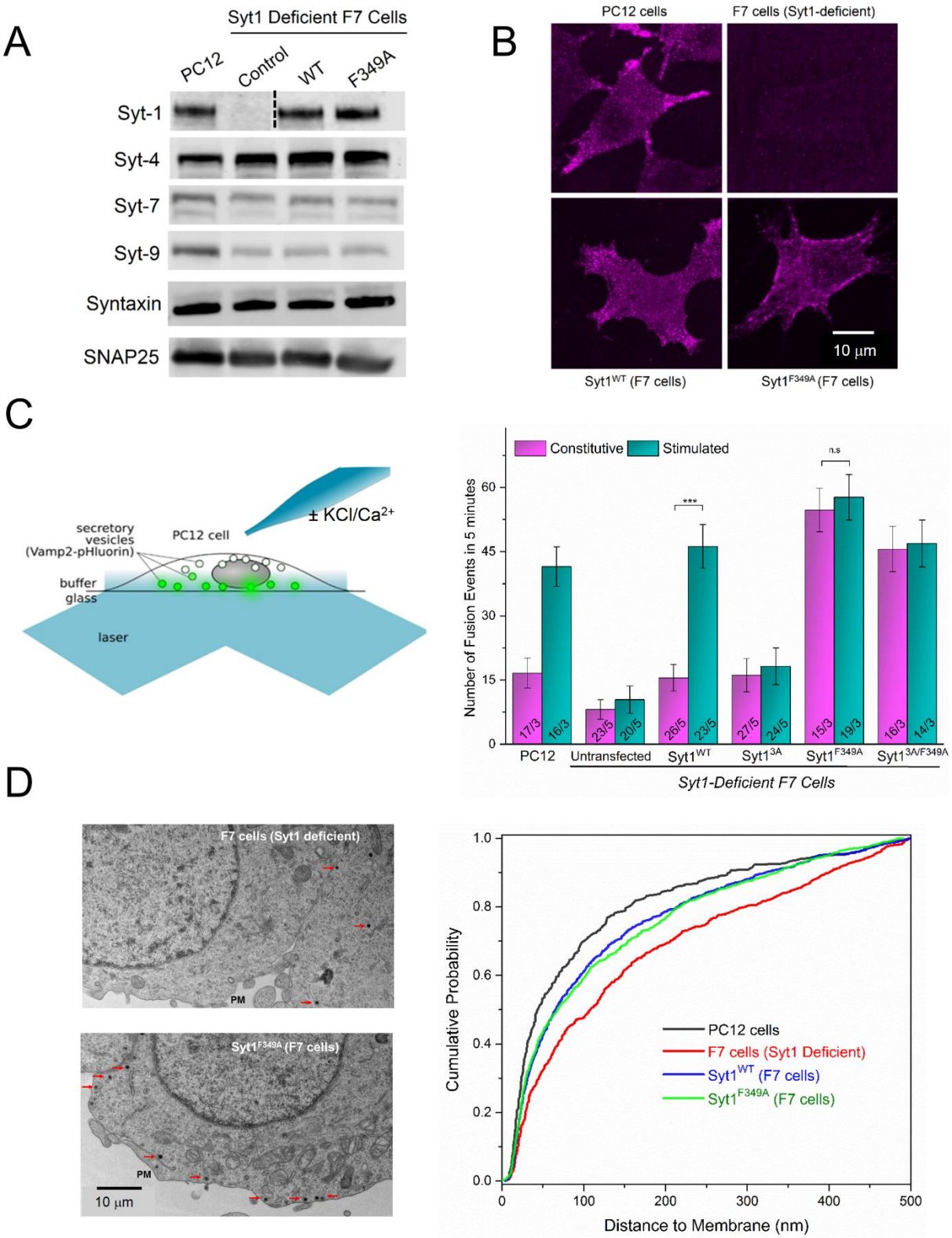
A
Syt1 Deficient F7 Cells
PC12
Control
WT
F349A
Syt-1
Syt-4
Syt-7
Syt-9
Syntaxin
SNAP25
B
PC12 cells
F7 cells (Syt1-deficient)
10 µm
Syt1WT (F7 cells)
Syt1F349A (F7 cells)
C
secretory vesicles (Vamp2-pHluorin)
PC12 cell
± KCl/Ca2+
buffer
glass
laser
Constitutive
Stimulated
n.s
***
Number of Fusion Events in 5 minutes
0
15
30
45
60
17/3
16/3
23/5
20/5
26/5
23/5
27/5
24/5
15/3
19/3
16/3
14/3
PC12
Untransfected
Syt1WT
Syt13A
Syt1F349A
Syt13A/F349A
Syt1-Deficient F7 Cells
D
F7 cells (Syt1 deficient)
PM
Syt1F349A (F7 cells)
PM
10 µm
Cumulative Probability
0.0
0.2
0.4
0.6
0.8
1.0
0
100
200
300
400
500
Distance to Membrane (nm)
PC12 cells
F7 cells (Syt1 Deficient)
Syt1WT (F7 cells)
Syt1F349A (F7 cells)

FIGURE 4

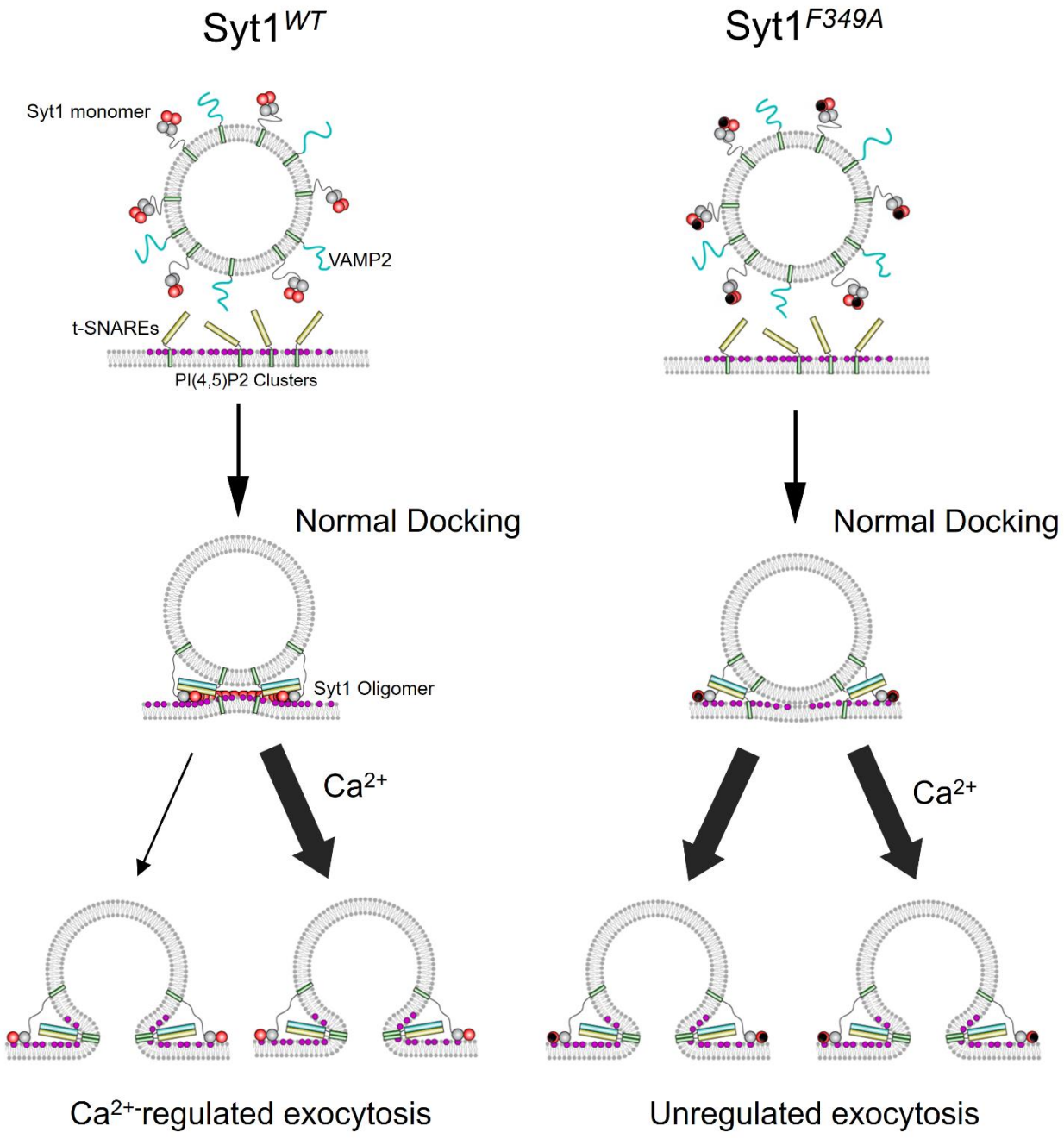
Syt1WT
Syt1F349A
Syt1 monomer
VAMP2
t-SNAREs
PI(4,5)P2 Clusters
Normal Docking
Normal Docking
Syt1 Oligomer
Ca2+
Ca2+
Ca2+-regulated exocytosis
Unregulated exocytosis

Supplementary Information

Synaptotagmin Oligomerization is Essential for Calcium Control of Regulated Exocytosis

Oscar D. Bello[a,b,1], Ouardane Jouannot[a,1], Arunima Chaudhuri[a], Ekaterina Stroeva[a], Jeff Coleman[a], Kirill Volynski[b], James E. Rothman[a,b,2] & Shyam S. Krishnakumar[a,b,2]

[a]Department of Cell Biology, Yale University School of Medicine, 333 Cedar St, New Haven, CT 06520 USA

[b]Department of Clinical and Experimental Epilepsy, Institute of Neurology, Queens Square House, University College London, London, WC1 3BG, UK.

[1]These authors contributed equally

[2]Correspondence: james.rothman@yale.edu; shyam.krishnakumar@yale.edu

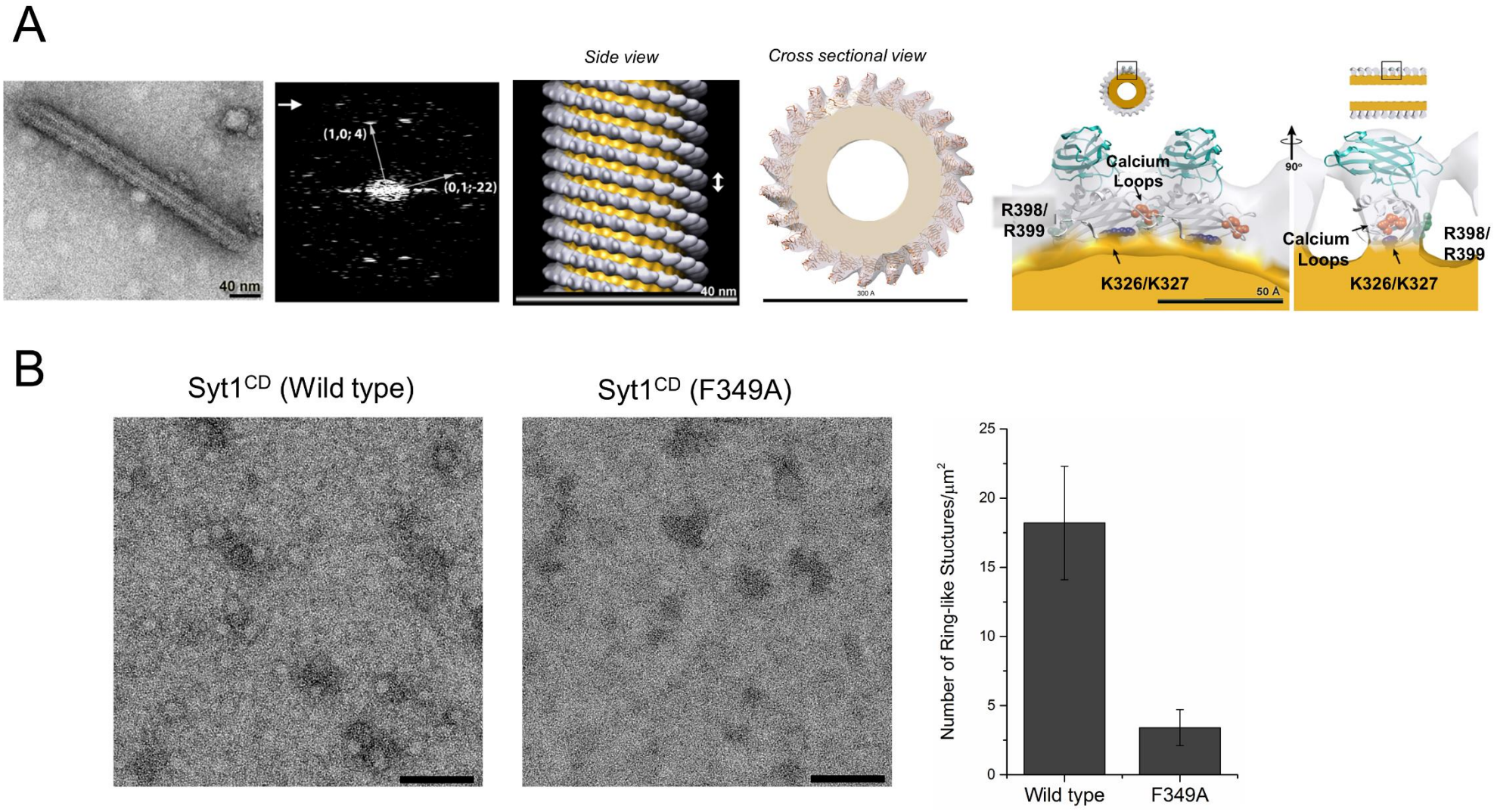

Figure S1. (A) Reconstruction of Syt1^{C2AB} coated lipid tubes adapted from Wang *et al*. 2014(19). Representative electron micrograph of Syt1^{C2AB} decorated lipid bilayer tube, as visualized by negative staining. Syt1 ring oligomer with similar diameter as the tube is typically found at the end of these tubules, suggesting the continuous stacking of the rings may pull the lipid monolayer into tubes.

Syt1^{C2AB} coated tube produces a distinct diffraction pattern, which yields a EM surface map based on helical-reconstruction. Both the side and cross-section view are shown wherein the lipid monolayer is colored yellow and the Syt1^{C2AB} in grey. The dimension of the protein density (4 nm x 4 nm) is consistent with a single Syt1^{C2AB} molecule. The X-ray structure of the C2AB domain of Syt1$^{(49)}$ can be fitted into the EM density and surface representation of the tube is sectioned to the thickness of a single strand of the helix to reveal the shape of individual asymmetric unit. The C2B domain (gray) appears to mediate both the membrane association and the ring assembly. The PS/PIP2 binding polybasic patch (K326, K327, blue) are packed against the membrane surface, whereas the Ca^{2+} loops localize to the protein-protein interface involved in ring formation. The C2A domain (cyan) projecting radially away from the membrane surface does not contribute to membrane binding or ring formation. The calcium loops (orange) locate to the dimer interface and the conserved, SNARE-binding motif (R398, R399 green) is accessible and free to bind the SNARE proteins. (B) Negative stain EM analysis carried out in physiological buffer (25 mM MOPS, 100 mM KCl, 1mM $MgCl_2$, 1mM DTT) and lipid (72%PC:25%PS:3%PIP2) composition confirms that the F349A mutation disrupts the ring oligomer formation of entire cytoplasmic domain of Syt1 (Syt1^{CD}, residue 96-421). Representative micrographs are shown and the summary data from 3 independent experiments (mean ± SD) are shown.

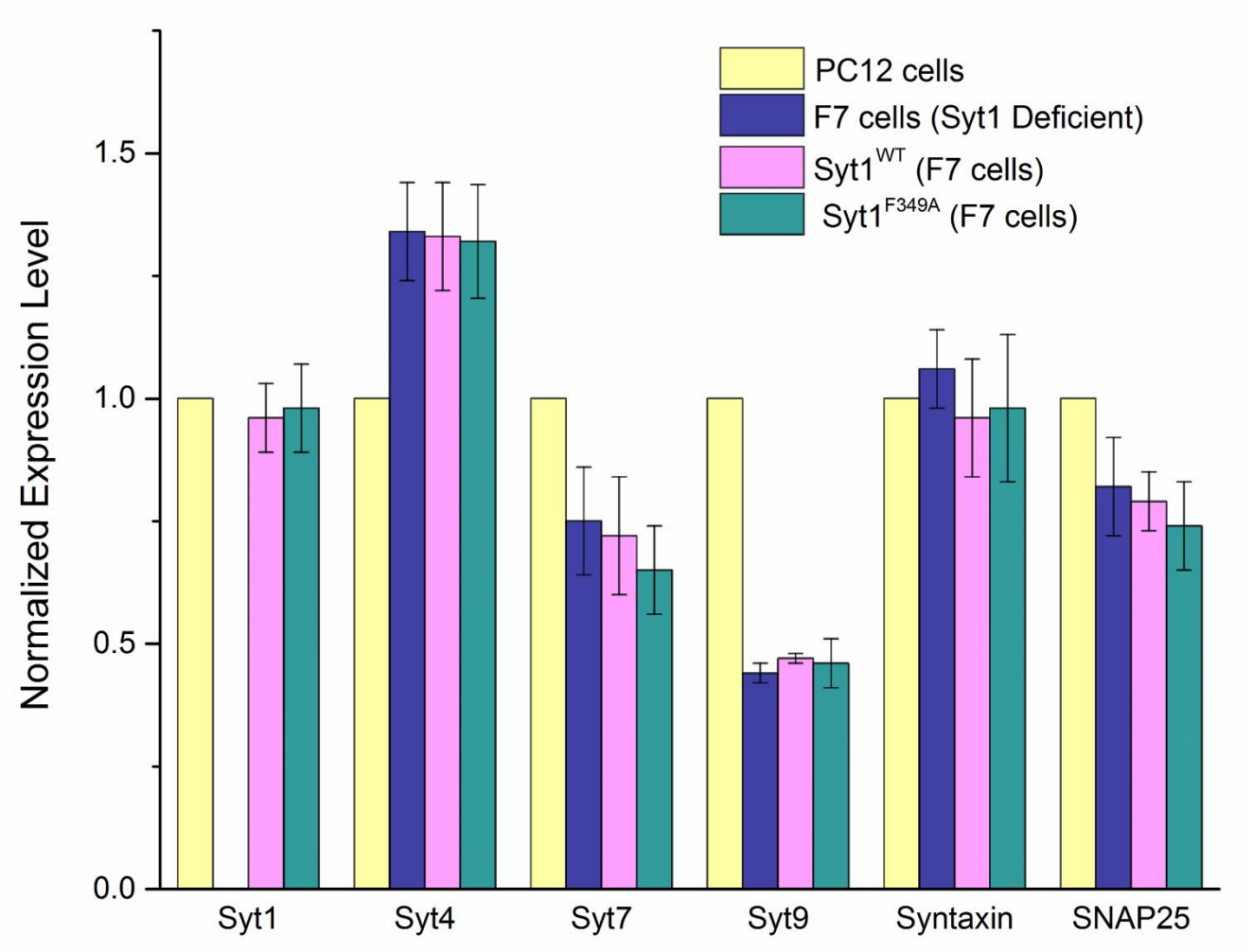

Figure S2. (A) Quantitation of protein expression levels examined by Western Blot analysis (Fig 2a) showing that untransfected F7 cells (blue bars) lack Syt1 and have ~50% reduction in Syt9 expression as compared to the normal PC12 cells (yellow). It further shows that recombinant $Syt1^{WT}$ and $Syt1^{F349A}$ proteins are expressed in transfected F7 cells at the levels comparable to the endogenous Syt1 in the control PC12 cells. It also confirms that the expression levels of the other Syt isoforms (Syt4, Syt7 and Syt9) or the t-SNARE proteins (Syntaxin-1 and SNAP25) are un-affected by overexpression of $Syt1^{WT}$ and $Syt1F^{349A}$ in F7 cells. Data are mean ± SD from 3 independent experiments, in all cases the expression levels were normalized to the endogenous levels in control PC12 cells.

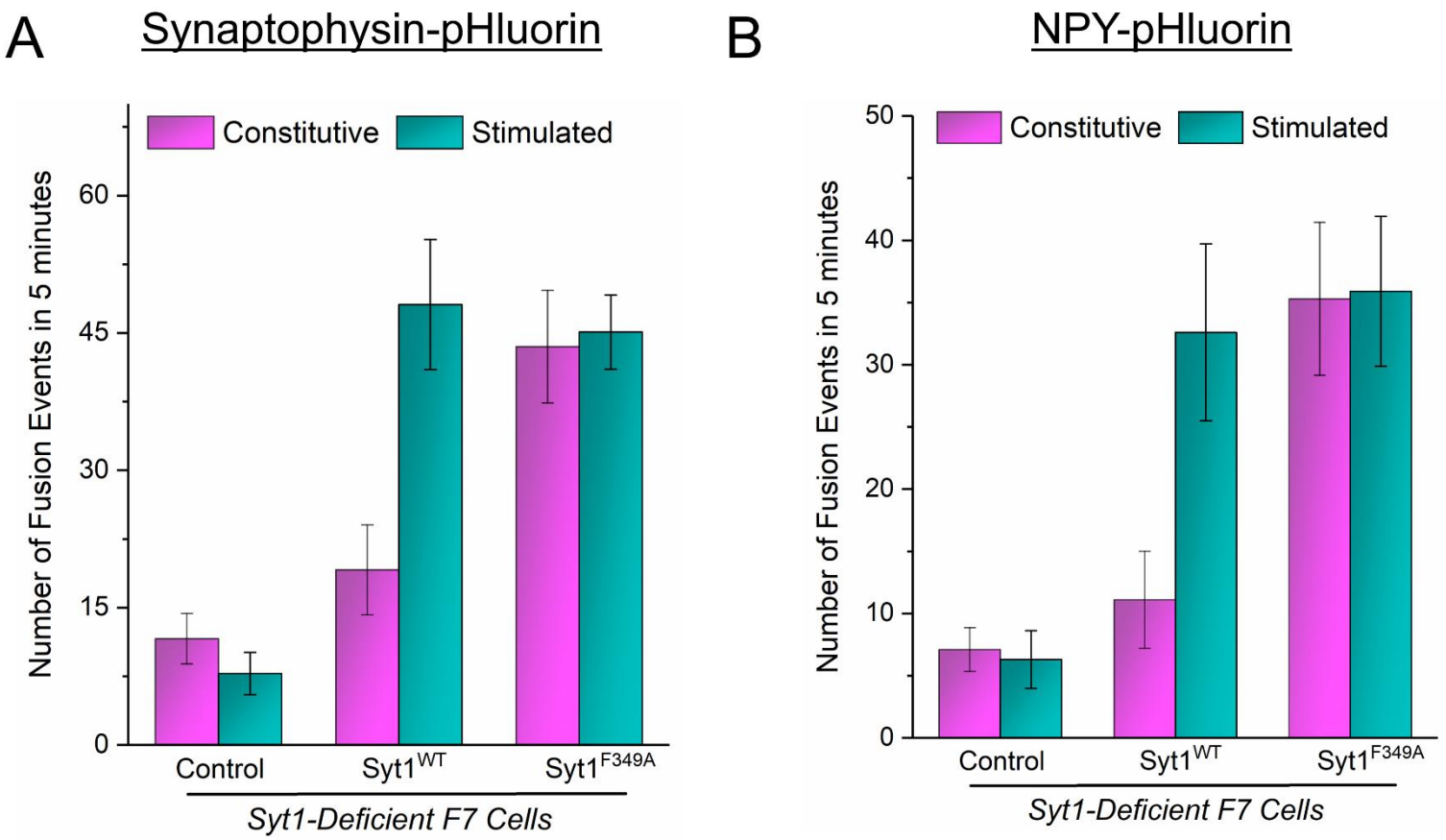

Figure S3. Effect on disrupting the Syt1 oligomerization using F349A mutation on the exocytosis of small, clear vesicles and large, dense core vesicles were assessed using the (A) Synaptophysin-pHluorin and (B) NPY-pHluorin (B) respectively. In both cases, single vesicle fusion events under basal (constitutive) and KCl-depolarized (Ca^{2+}-stimulated) conditions were imaged using TIRF microscopy. Consistent with the universal VAMP2-pHluorin marker (Fig. 3C), $Syt1^{F349A}$ expression specfically enhances the basal, constitutive fusion and occludes Ca^{2+}-control of neuroexocytosis when compared to $Syt1^{WT}$ transfected F7 cells for both the independent vesicle markers. These result further supports the notion the observed phenotype is specifically caused by disruption of C2B-dependent Syt1 oligomerization and is not due to off-target effect of $Syt1^{349A}$ expression.